ADVANCED MATERIALS INTERFACES
Open Access
www.advmatinterfaces.de

Enhanced Photoresponse in Intermingled WS_2 and MoS_2 Nanodiscs on Graphene Heterostructure Nanohybrids

Samar Ghopry, Andrew Shultz, Mohammed Alamri, Saad Alzahrani, and Judy Wu**

Nanohybrids based on van der Waals (vdW) heterostructures of two dimensional (2D) atomic materials have recently emerged as a unique scheme for designing high-performance quantum sensors. This work explores vdW nanohybrids for photodetection, which consist of graphene decorated with intermingled transition-metal dichalcogenide (TMDC) nanodiscs (TMDC-NDs) obtained using wafer-size, layer-by-layer growth. The obtained TMDC-NDs/graphene nanohybrids take advantage of strong quantum confinement in graphene for high charge mobility and hence high photoconductive gain, and localized surface plasmonic resonance (LSPR) enabled on the TMDC-NDs for enhanced light absorption. Since the LSPR depends on the nanostructure's size and density, intermingled TMDC-NDs of different kinds of TMDCs, such as WS_2 (W) and MoS_2 (M), have been found to allow small-size, high-concentration TMDC-NDs to be achieved for high photoresponse. Remarkably, high photoresponsivity up to 31 A/W (550 nm wavelength and 20 μW cm^{-2} light intensity) has been obtained on the WMW-NDs/graphene nanohybrids photodetectors made using three consecutive coatings of WS_2 (1st and 3rd coating) and MoS_2 (2nd coating), which is considerably higher by a factor of ≈4 than that of the counterparts MoS_2-ND/graphene or WS_2-NDs/graphene devices. This result provides a facile approach to control the size and concentration of the TMDC-NDs for high-performance, low-cost optoelectronic device applications.

1. Introduction

Two dimentional (2D) atomic materials like graphene and transition-metal dichalcogenides (TMDCs, such as WS_2 and MoS_2) have attracted intensive research interest lately as potential candidate materials for electronics and optoelectronics. 2D atomic materials have promising electronic and optical properties stemming from their unique electronic structures under 2D quantum confinement.[1] For example, MoS_2 exists in nature as an n-type semiconductor with an indirect bandgap while monolayer MoS_2 (WS_2) has a direct bandgap hence stronger light absorption than its bulk counterpart in the visible spectrum[1d,2] to near-infrared with carrier doping.[3] 2D MoS_2 (WS_2) has a visible-range bandgap ranging from 1.6–1.9 eV for monolayer layer[4] to 1.2–1.4 eV for multilayers.[4a,b,5] On the other hand, graphene is well known for its high carrier mobility due to its unique gapless Dirac cone electronic structure and the linear dispersion associated to its hexagonal 2D lattice of carbon atoms of 0.34 nm in thickness, leading to extraordinary mobility for massless fermions (electrons and holes).[6] At room temperature, the mobility of graphene, up to 2 × 10^5 cm^{-2} V^{-1} s^{-1}, plays a critical role in providing photoconductive gain.[7] In addition, graphene has ≈2.3% absorption per sheet in broadband ranging from ultraviolet (UV) to almost terahertz, which represents the highest light absorption so far observed per atomic sheet.[8] Furthermore, 2D atomic materials and their heterostructures can have excellent mechanical strength and stability required for flexible electronic devices.[9]

Photodetectors based on TMDC have been studied intensively and promising progress has been obtained. For example, photoresponsivity of ≈0.42 mA W^{-1} was reported on a monolayer MoS_2 phototransistor at incident light power of (P_{light}) of 80 μW,

S. Ghopry
Department of Physical Sciences
Physics Division, College of Science
Jazan University
P.O. Box 114, Jazan 45142, Kingdom of Saudi Arabia
E-mail: sghopry@jazanu.edu.sa

The ORCID identification number(s) for the author(s) of this article can be found under https://doi.org/10.1002/admi.202500087

DOI: 10.1002/admi.202500087

S. Ghopry
Nanotechnology Research Unit
Jazan University
P.O. Box 114, Jazan 45142, Kingdom of Saudi Arabia

A. Shultz, S. Alzahrani, J. Wu
Department of Physics and Astronomy
University of Kansas
Lawrence, KS 66045, USA
E-mail: jwu@ku.edu

M. Alamri
Department of Physics
Umm Al-Qura University
Makkah 24381, Kingdom of Saudia Arabia

a wavelength of 550 nm and a source-drain bias voltage (V_{ds}) of 1.0 V.[2b] By applying a gate voltage of ≈50 V, the photoresponsivity reaches 7.5 mA W^{-1}. Lan et al synthesized a photodetector based on large-area monolayer WS_2 films prepared using chemical vapor deposition (CVD) and obtained photoresponsivity of 0.2 μA W^{-1} at a wavelength of 532 nm and rise and fall times of ≈ 4.5 ms.[10] The relatively low photoresponsivity in photodetectors based solely on TMDC has prompted exploration of van der Waals (vdW) heterostructures of TMDC and graphene to incorporate a large photoconductive gain for higher photoresponsivity.[1e] TMDC and other 2D materials of different electronic structures and doping (p or n types) can be stacked together into vdW heterostructures to enable broadband optoelectronics with favorable band-edge alignments at the interfaces.[11] These advantages have motivated a large number works to explore vdW p-n junctions, such as $MoTe_2/MoS_2$,[12] WSe_2/MoS_2,[13] WSe_2/SnS_2[14] black phosphorous (BP)/MoS_2,[15] GaTe/InSe,[16] WS_2/MoS_2,[17] and h-BN/$MoTe_2$/graphene/SnS_2/h-BN[18] for photodetection. In TMDC/graphene vdW nanohybrids, a high photoconductive gain stemming from the strong quantum confinement in TMDC (as photosensitizer) and graphene (as charge transport channel) may be achieved for extraordinary photoresponsivity. The gain can be estimated from the ratio between the exciton time ($\tau_{exciton}$) in TMDCs and the charge transit time ($\tau_{transit}$) in graphene.[19] High-performance TMDC/graphene vdW nanohybrid photodetectors have been reported.[20] For example, an 835 mA W^{-1} photoresponsivity in visible spectrum has been reported for a printed MoS_2 sheet on transfer-free wafer-size graphene.[20b] A further enhanced visible photoresponsivity by decorating WS_2 nanodiscs (NDs) on graphene was reported by Alamri et al[21] and the enhancement was attributed to the generation of localized surface plasmonic resonance (LSPR) on WS_2 NDs upon light illumination for improved light absorption and hence photoresponsivity.[22]

Since TMDC-NDs with the LSPR effect can effectively enhance light absorption, a further enhanced photoresponsivity is anticipated by increasing the TMDC-NDs concentration, which presents a challenge due to the requirement of maintaining the optimal ND size around 100s of nm. Motivated by this, this work explores schemes to increase the TMDC-ND concentration by using multiple consecutive coatings of the same kind and different kinds of TMDCs. The former only led to larger, thicker, and even connected TMDC-NDs with a negligible increase in ND concentration. In contrast, the latter was found to allow formation of intermingled TMDC-NDs of enhanced concentrations while maintaining similar lateral sizes TMDC-NDs in the range of 300 to 500 nm. Significantly enhanced photoresponsivity by ≈400% has been obtained in the intermingled TMDC-NDs/graphene vdW heterostructure nanohybrids photodetectors as compared to their counterparts of only one kind of TMDC-NDs.

Figure 1 exhibits two different photodetectors based on TMDC-NDs/graphene vdW heterostructures. One has one kind of TMDC-NDs, such as MoS_2-NDs or WS_2-NDs (Figure 1a), and the other has intermingled TMDC-NDs from different kinds of TMDCs such as WS_2 (W) and MoS_2 (M). Figure 1b shows one such example of WM-NDs/graphene generated with two consecutive coatings of MoS_2 (1st coating) and WS_2 (2nd coating). While the TMDC-NDs have comparable dimensions in the two cases, the latter could have a higher TMDC-ND concentration

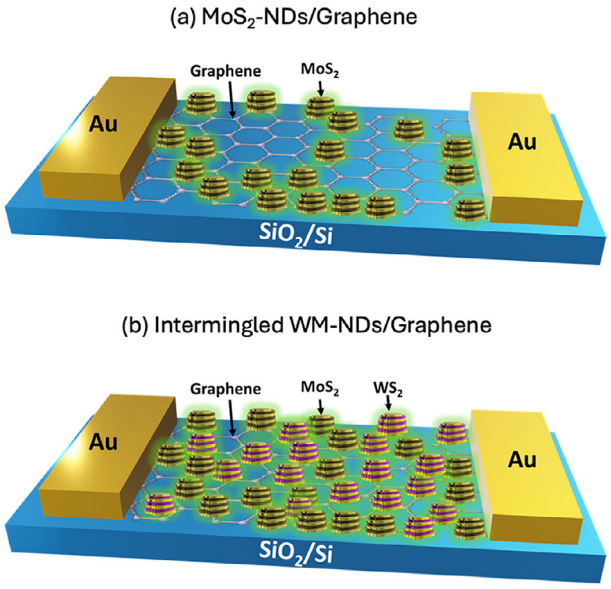

Figure 1. Schematics illustration of TMDC-NDs/graphene vdW nanohybrids photodetectors with: a) one coating of MoS_2-NDs, and b) two consecutive coatings of MoS_2-NDs (first coating, black/gold) and WS_2-NDs (second coating, purple/gold) to obtain an intermingled WM-NDs/graphene nanohybrid.

to allow enhanced light absorption and hence photoresponsivity in the TMDC-NDs/graphene nanohybrids photodetectors. Under the light illumination, the photoexcited electron–hole pairs (excitons) are created in the TMDC-NDs and separated to free charge carriers with assistance of the built-in electric field due to the band edge alignment between TMDC and graphene at the TMDC/graphene interface.[20b] This interface is also important to the observed LSPR effect in the TMDC-NDs based on density functional theory simulation.[22b] For optoelectronic devices, enhanced light absorption in TMDC-NDs, as compared with continuous TMDC sheets, can lead to improved performance as shown previously in photodetectors[21] and biosensors.[22]

Figure 2a,b exhibits Raman spectra of MoS_2 on the MoS_2-NDs/graphene and WS_2 on WS_2-NDs/graphene nanohybrids respectively. In the Raman spectrum of MoS_2, the two peaks can be assigned to the E^1_{2g} at ≈384 cm^{-1} and $A_{1\ g}$ at ≈409 cm^{-1} bands of MoS_2. Similarly, the Raman spectrum of WS_2 also exhibits two peaks assigned to the E^1_{2g} at ≈367 cm^{-1} and $A_{1\ g}$ at ≈424 cm^{-1} bands of WS_2. Figure 2c,d shows Raman maps of the $A_{1\ g}$ band measured on MoS_2-NDs/graphene samples with one or two consecutive coatings of MoS_2, respectively. In both samples, MoS_2-NDs can be clearly seen while their morphology and concentration differ. In the sample with one coating, the MoS_2-NDs are rounded in shape with lateral size of 300–500 nm. The concentration of MoS_2-NDs is ≈0.43 particles μm^{-2} (Figure 2c). Figure S1 (Supporting Information) shows the optical microscopy and Raman spectra and maps taken on several different spots over a large piece of MoS_2-NDs/graphene sample of 1 × 2.5 cm^2 in dimension (limited by the furnace tube size in the lab). The formation of the MoS_2-NDs is fairly uniform over the sample area covered with graphene.

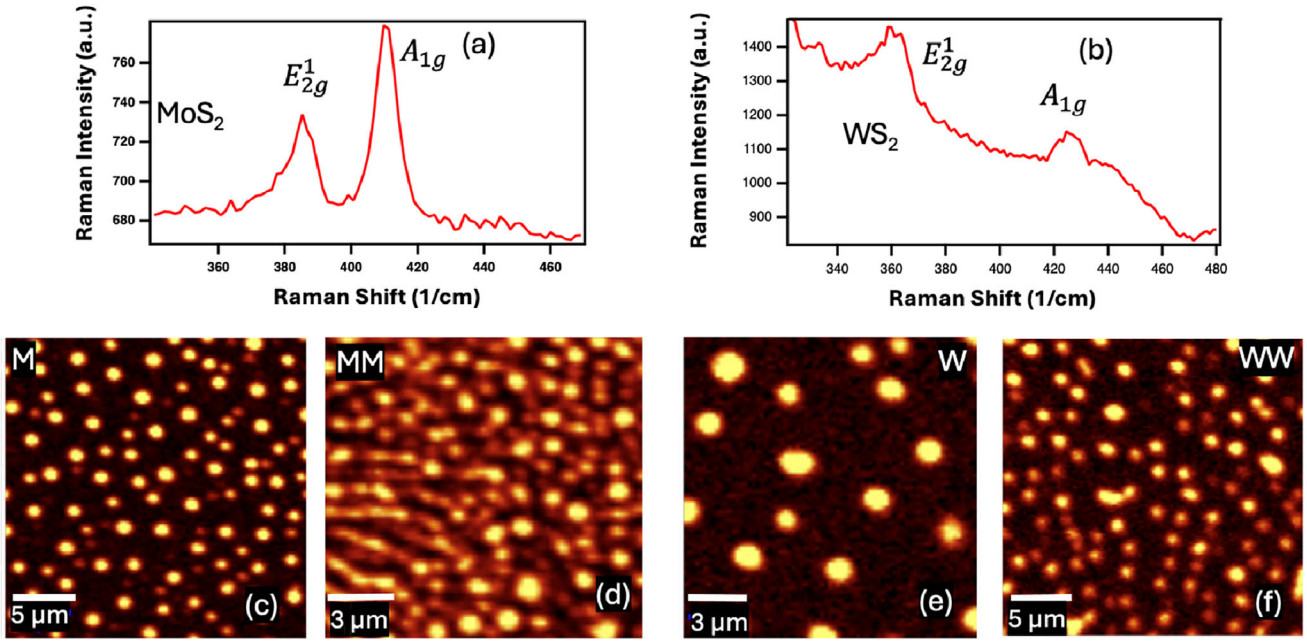

Figure 2. Raman spectra of MoS_2-NDs a) and WS_2-NDs b). Raman maps of c) MoS_2-NDs fabricated with one coating of MoS_2 and d) MM-NDs fabricated with two consecutive coatings of MoS_2. Raman maps of e) WS_2-NDs fabricated with one coating of WS_2 and f) WW-NDs fabricated with two coatings of WS_2. All Raman maps were taken using the TMDC A_{1g} peak. A Raman excitation laser of 488 nm wavelength was used.

Adding an additional coating of MoS_2 on this sample, namely, MM-NDs in Figure 2d leads to connected MoS_2-NDs or MoS_2 stripes of lengths up to 5–10 μm in addition to NDs with lateral size of ≈450 nm. Figure 2e-f compares the Raman maps of WS_2 A_{1g} band on WS_2-NDs (one coating) and WW-NDs (two consecutive coatings), respectively. While the WS_2-NDs in these two samples have a similar rounded shape, their morphology differs from that of the MoS_2-NDs in Figure 2c. For example, the WS_2-NDs sample has a lower ND concentration ≈0.13 particles μm^{-2} and larger lateral size of 600 nm–1.1 μm. Interestingly, adding one more coating of WS_2 (Figure 2e) shows higher WS_2-NDs concentration ≈ 0.29 particles μm^{-2} while a slightly reduced ND size of ≈ 350–800 nm.

The results shown in Figure 2 suggest that two consecutive coatings of the same kind of TMDC may not allow small-size and high-concentration TMDC-NDs to be achieved. Even though the NDs in the WW-NDs sample have smaller size and higher concentration than that in the W-NDs sample, they are not as good as those in the MoS_2-NDs sample. In order to resolve this issue, intermingled TMDC-NDs were explored assuming dis-similar chemistries in different kinds of TMDCs would make ND nucleation preferred on open areas not occupied by the other kinds of TMDC-NDs.

Figure S2a (Supporting Information) displays the Raman spectra taken on six samples of pristine graphene only (pink), WS_2-NDs/graphene (blue),[22a] MoS_2-NDs/graphene (orange), Au nanoparticles (NPs)/graphene (green),[22a] WS_2+AuNps/graphene (red)[22a] and on MW-NDs/graphene (black), which has graphene's three peaks of D at ≈1356 cm^{-1}, G at ≈1587 cm^{-1}, and 2D at ≈2695 cm^{-1}. On the graphene-only sample, the ratio of the graphene 2D/G peak intensities is ≈1.9. In addition, the defect D band intensity is negligibly small, indicating that the graphene is high-quality monolayer. On samples with plasmonic nanostructures decorated on graphene, significantly enhanced peak intensities of graphene can be observed. Nevertheless, the enhancement differs quantitatively on the 5 samples, indicating different LSPR effects induced by the decorated plasmonic nanostructures. Figure S2b (Supporting Information) shows the corresponding calculated enhancement factors of the graphene peaks (G and 2D) on different samples (normalized to the intensity of the peak on the graphene-only sample). Specifically, the G and 2D peaks are enhanced by a factor of 3.5 and 2.7 on WS_2-NDs/graphene (blue), and 4.3 and 3.0 on MoS_2-NDs/graphene. Interestingly these enhancement factors are similar to that reported on plasmonic metal nanostructures/graphene.[23] For example, the enhancement factors of 5.4 and 4 for G and 2D peaks were observed on the AuNPs/graphene (green). On the AuNP/WS_2-NDs/graphene sample, the enhancement factors of the graphene G and 2D peaks are 7.9 and 5.6, respectively, which may be attributed to the superposition of the LSPR effects of AuNPs and WS_2-NDs. Therefore, the higher enhancement factors of the G and 2D peaks around 6.1 and 4.2 on MW-NDs/graphene (black) than that in the WS_2-NDs/graphene and MoS_2-NDs/graphene can be regarded as the superposition of the LSPR effects from the two kinds of TMDC-NDs in the MW-NDs/graphene. Note the LSPR enabled on TMDCs-NDs is comparable or slightly higher than that by AuNPs, which indicates the photodoping associated with the strong dipole-dipole interaction at the heterostructure interface revealed by the DFT and AMID simulations can be effective to induce LSPR on TMDC-NDs/graphene.[22] **Figure 3a–g** shows the Raman spectrum and Raman maps taken on a WM-NDs/graphene sample made with two consecutive coatings of MoS_2 (first coating) and WS_2 (second coating). The Raman

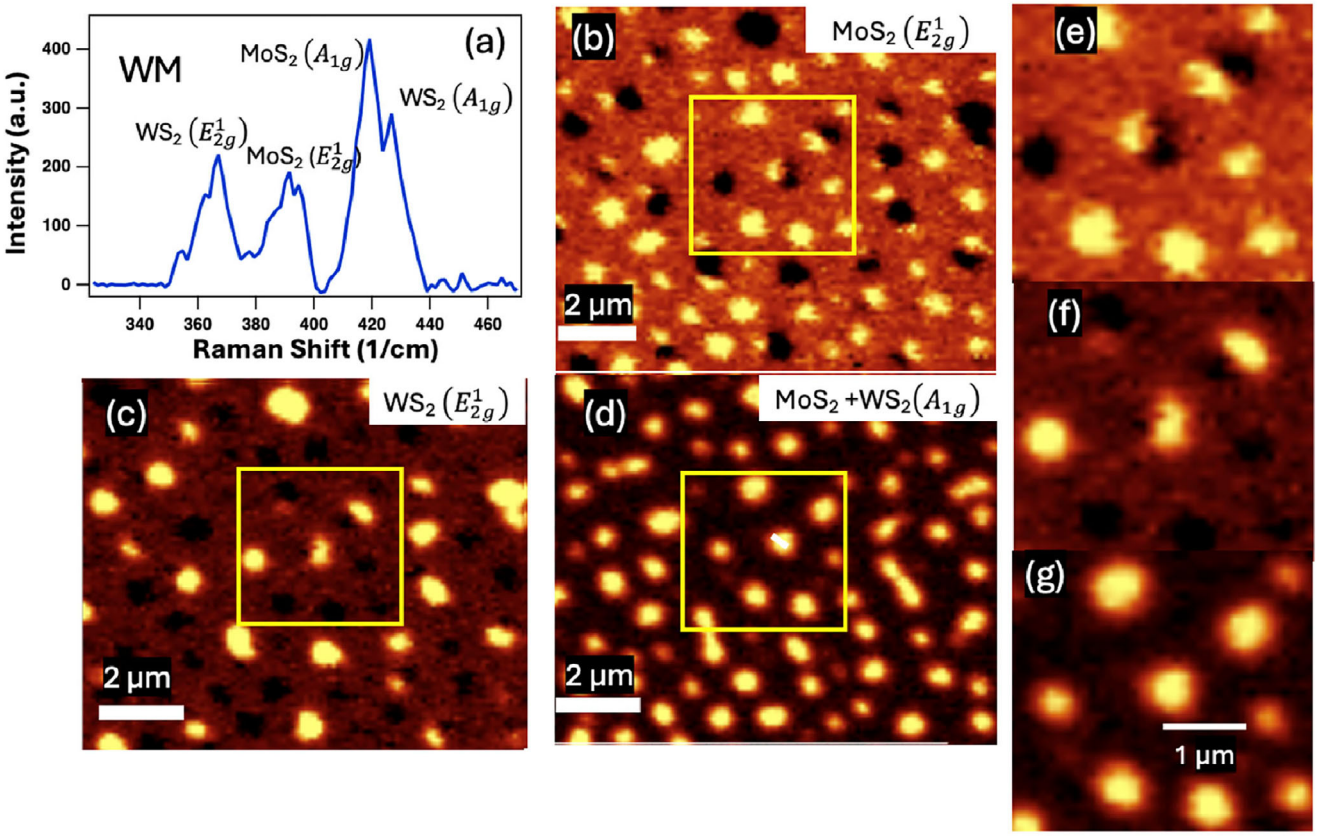

Figure 3. Raman spectrum a) and Raman maps b–d) of WM-NDs made with two consecutive coatings of MoS_2 (1st coating) and WS_2 (2nd coating). In the Raman maps, the E^1_{2g} peaks were used for MoS_2 b) and WS_2 c) respectively and the A_{1g} peaks, for both MoS_2 and WS_2 in d). e–g) Zoom-in views of the Raman maps in the squared areas of b–d), respectively.

spectrum of WM-NDs shows four peaks that assigned to the E^1_{2g} at ≈394 cm^{-1} and A_{1g} at ≈419 cm^{-1} modes of MoS_2 and to the E^1_{2g} at ≈367 cm^{-1} and A_{1g} at ≈424 cm^{-1} modes of WS_2, which confirms that both WS_2 and MoS_2 are present in the WM-ND sample. Figure 3b,c exhibits the Raman maps of the WS_2 (E^1_{2g} mode) and MoS_2 (E^1_{2g} mode), respectively. The contrast in the brightness demonstrates clearly that most WS_2-NDs and MoS_2-NDs are located at different locations in the WM-NDs/graphene samples, instead of being on top of each other. This morphology (small size as well as uniform and large concentration) is improved when compared to that on samples made from repeated coatings of the same types of TMDC-NDs. Figure 3d shows the Raman A_{1g} peaks map for MoS_2 and WS_2 together (since the two A_{1g} peaks are very close to each other) and illustrates the TMDC-ND morphology for the WS_2-NDs and MoS_2-NDs with the density of 0.69 particles μm^{-2} and size of 270–550 nm. Figure 3e–g shows the zoomed-in Raman maps in the area indicated by the square in Figure 3b–d.

Furthermore, the MW-NDs/graphene samples with an opposite coating order of WS_2 (1st coating) and MoS_2 (2nd coating) were also fabricated. Figure S3 (Supporting Information) compares the Raman maps of WM-NDs (on the top) and MW-NDs (on the bottom). In the WM-NDs sample, both MoS_2-NDs (first coating) and WS_2-NDs (second coating) grow uniformly with M-ND size of 250–500 nm, and the W-NDs, grown in the gaps between M-NDs, of size 300–600 nm. In the MW-NDs sample, WS_2 (first coating) grows with varied sizes 500–1200 nm and when coating MoS_2 (second coating) M-NDs grow covering the wide gap area with very small size ≈300 nm and high density. In general, alternative coatings of different kinds of TMDCs lead to improved TMDC-ND size and density on both samples of MW-NDs and WM-NDs (Figure S3c–f, Supporting Information). Quantitively, the TMDC-NDs size is 410 ± 130 nm, and density of 0.69 particles μm^{-2} in the Sample WM-NDs/graphene. In the MW-NDs sample, the TMDC-ND size and density are respectively ≈400 ± 200 nm and 0.96 particles μm^{-2}. **Figure** 4a–d compares the Raman spectra (on top) and Raman maps (at bottom) of four TMDC-NDs/graphene samples with: M-NDs (one coating), WM-NDs made with two consecutive coatings of MoS_2 (1st coating) and WS_2 (2nd coating), MWM-NDs made with three consecutive coatings MoS_2 (1st coating), WS_2 (2nd coating), and MoS_2 (3rd coating), and WMW-NDs made WS_2 (1st coating), MoS_2 (2nd coating), and WS_2 (3rd coating), respectively. The additional coatings in the samples with MW-NDs, MWM-NDs, and WMW-NDs have shown higher TMDC-NDs concentrations than those in the MoS_2-NDs/graphene sample. While a few larger-size NDs are visible in the multi-coating samples, the majority of TMDC-NDs have comparable size to that in the single-coating MoS_2-NDs

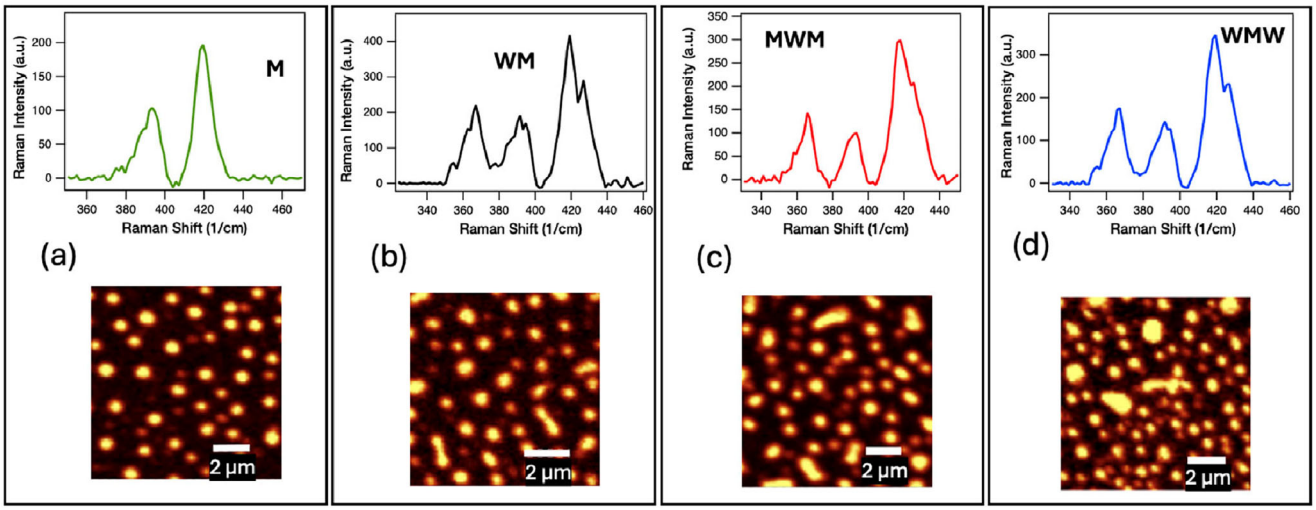

Figure 4. Raman spectra (on top) and Raman maps (on bottom) of a) M-NDs made with one coating of MoS_2, b) WM-NDs made with two consecutive coatings of MoS_2 (1st coating) and WS_2 (2nd coating), c) MWM-NDs made with three consecutive coatings of MoS_2 (1st coating) and WS_2 (2nd coating) and MoS_2 (3rd coating), and d) WMW made three consecutive coatings of WS_2 (1st coating) and MoS_2 (2nd coating) and WS_2 (3rd coating)) on graphene. All Raman maps were collected using the TMDC A_{1g} peaks. A Raman excitation laser of 488 nm wavelength was used.

samples, suggesting intermingled MoS_2-NDs and WS_2-NDs can be obtained using consecutive coatings of different TMDC-NDs.

Figure 5 summarizes the variation of the TMDC-NDs concentration (blue) and size (red) in a set of TMDC-NDs/graphene samples synthesized using either single or multiple coatings of TMDC-NDs. With increasing number of TMDC-NDs coatings, the TMDC-NDs concentration increases approximately monotonically from ≈0.13 ± 0.03 particles μm^{-2} and 0.44 particles μm^{-2}, respectively, for the single-coating W-NDs and M-NDs to 1.1 ± 0.1 particles μm^{-2} for the WMW-NDs. Interestingly, the increase of the TMDC-ND concentration with increasing number of coatings of the same kinds of TMDC is moderate or even reversed. For example, the concentrations for the M-NDs of 0.44 particles μm^{-2} concentration decrease to 0.12 particles μm^{-2} on MM-NDs. The concentration increases only slightly from W-NDs to WW-NDs, and both have a fairly low ND concentration below 0.40 particles μm^{-2}. In contrast, the alternative coatings of different kinds of TMDC-NDs in the four samples on the right side of Figure 5 lead to a considerable increase of the TMDC-NDs concentration. This suggests that alternating different kinds of TMDC-NDs coatings may prevent continuous growth of the

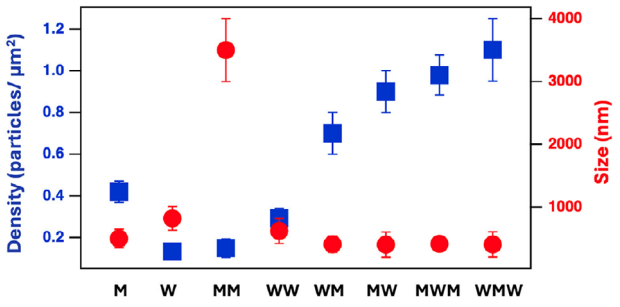

Figure 5. Average density (blue) and average size (red) of the TMDC-NDs as a function of the TMDC coating structures of the samples. Error bars represent the standard deviation of the measurement.

formed NDs to large size and thickness. This argument is supported by the trend of TMDC-ND size in Figure 5. Basically, the W-NDs and WW-NDs have the largest diameters of 700–1100 nm among the eight samples in Figure 5 while the other six samples have approximately comparable size. In particular, the four samples on the right side of Figure 5 with two or three alternative TMDC-NDs coatings have ND size of 400–600 nm. Therefore, the intermingled TMDC-NDs/graphene samples show higher ND concentration and smaller ND size as compared to the samples made with one or two coatings of the same kind of TMDCs. While understanding the ND nucleation mechanism requires further investigation, we hypothesize that the formation of small TMDC-NDs in the starting coating would assist the different kinds of TMDC-ND to nucleate away from or at the gap between the existing NDs, resulting in higher concentration and smaller size of intermingled TMDC-NDs on graphene.

Figure S4 (Supporting Information) compares three optical absorption spectra in the wavelength range of 300–900 nm taken on the TMDC-NDs/graphene nanohybrids including MoS_2-NDs (blue), MM-NDs (red) and WM-NDs (two alternative coatings, black) on glass substrates. The absorption of the WM-NDs has the highest value among the three samples, demonstrating the advantage of the intermingled TMDC-NDs approach to prevent formation of large-size, low-concentration TMDC-NDs. For example, at 550 nm wavelength, the absorption in the WM-NDs/graphene is 1.5 higher than that in the M-NDs/graphene sample. Interestingly, the M-NDs/graphene and MM-NDs/graphene samples have comparable absorption despite the latter has two coatings of the precursor and is expected to have twice the amount of MoS_2, indicating the shape and dimension of the NDs play a critical role in light absorption. It should be noted that although the TMDC-NDs have significantly higher light absorption than their counterparts of TMDC continuous layers due to the LSPR effect in the former, the LSPR enhancement decreases with increasing TMDC-ND dimension and diminishes when dimension of TMDC-NDs

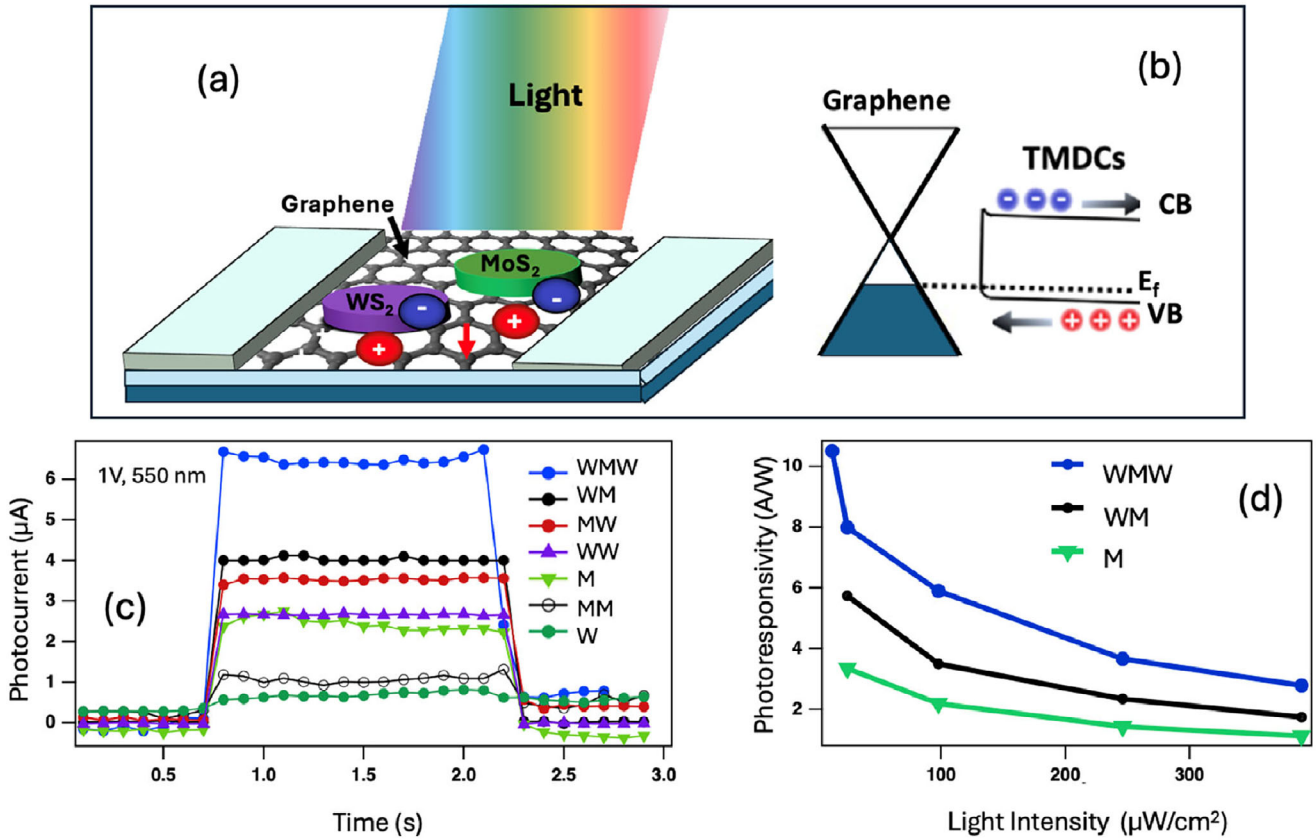

Figure 6. a) Schematic illustration of the optoelectronic process in a TMDC-NDs/graphene vdW nanohybrids photodetector. b) Band-edge alignment at the TMDC-NDs/graphene interface. c) Dynamic photoresponse measured with seven TMDC-NDs/graphene devices of different TMDC-NDs including W-NDs, M-NDs, MM-NDs, WW-NDs, MW-NDs, WM-NDs, and WMW-NDs (light wavelength: 550 nm and light power: 0.4 mW). d) Photoresponsivity as a function of the incident light intensity on the three TMDC-NDs/graphene nanohybrid devices with: WMW-NDs, WM-NDs, and M-NDs respectively. V_{sd} = 1.0 V for all measurements.

exceeds ≈1000 nm and when the concentration is low.[22b] The absorption spectra of the two TMDC-NDs/graphene nanohybrids samples each exhibit two broad and shallow shoulders at wavelengths of 400–450 and 550–600 nm, respectively, which are attributed to the LSPR wavelength of the WS_2-NDs and MoS_2-NDs.[22]

Figure 6a shows the device schematics of the TMDC-NDs/graphene vdW nanohybrids photodetectors with the band-edge alignment at the TMDC-NDs/graphene interface (Figure 6b). When the light is absorbed by the TMDC-NDs, the excitons (or electron-hole pairs) generated in the TMDC-NDs are expected to dissociate to free electrons and holes followed with transfer of one type of charges from TMDC-NDs to graphene with assistance of the interface build-in electric field. It should be noted that the CVD graphene is commonly p-doped due to the adsorbed polar molecules such as H_2O and O_2 on graphene in ambient, which leads to a downshift of the Fermi energy of graphene as illustrated schematically in Figure 6b.[24] This means that hole transfer is more favorable across the TMDC-NDs/graphene interface. The electrons would remain trapped in the TMDC-NDs before they recombine with holes, resulting in photogating effect on graphene channel.[25] Figure 6c compares the dynamic photoresponse measured in response to an on-and-off of visible light of 550 nm in wavelength measured on seven TMDC-NDs/graphene nanohybrids photodetectors. While all samples have graphene, they have different TMDC-NDs including W-NDs, M-NDs, MM-NDs, WW-NDs, MW-NDs, WM-NDs, and WMW-NDs. Since the same light intensity of 0.4 mW and V_{sd} = 1.0 V were applied to all seven samples, the amplitudes of the photoresponse reflect the differences associated to the different TMDC-NDs in these samples. Interestingly, the TMDC-NDs/graphene devices with intermingled MW-NDs (red), WM-NDs (black), and WMW-NDs (blue) exhibit higher photoresponse than that with the same kinds of TMDC-NDs either with single or double coatings. The highest photoresponse was observed on the WMW-NDs/graphene photodetector. Comparing devices with one coating of TMDC-NDs, such as M-NDs (light green) and W-NDs (dark green), and two coatings of the same TMDC-NDs, such as MM-NDs (open black) and WW-NDs (purple), the trend of photoresponse variation seems to correlate closely with the TMDC-NDs morphology. In the case of M-NDs/graphene and MM-NDs/graphene, the NDs become asymmetric and larger (average of width and length of the strips) in the latter with a comparable ND concentration to that of the former, which leads to a reduced photoresponse in MM-NDs/graphene. In contrast, the ND dimension reduces, and

concentration increases in the devices with WW-NDs/graphene as compared to the W-NDs/graphene case, which results in higher photoresponse in the former.

Figure S5a (Supporting Information) shows dynamic photoresponse under multiple lights (550 nm wavelength) on and off cycles measured on the WMW-NDs/graphene sample. Despite a moderate fluctuation of the amplitude of the photoresponse, the sample exhibits good cycling stability. Figure S5b (Supporting Information) illustrates a zoom-in view of the photoresponse for estimation of the rise (t_{rise}) and fall times (t_{fall}), defined as the required time for photoresponse to rise from 10% to 90% of its maximum and fall from 90% to 10%, respectively.[26] The t_{rise} and t_{fall} for this sample and also the other samples in Figure 4c are in the range of 10 and 20 ms, which are comparable to that measured on a continuous bilayer of MoS_2/graphene[20b] It should be noted that a slower response by more than an order of magnitude was reported on nanohybrids made by transferring MoS_2 flakes on graphene,[27] indicating direct growth of MoS_2, either continuous layer or NDs as reported in this work, provides benefits of reduced interface charge traps that decreases the photoresponse and response speed. However, further improvement to eliminate charge traps on the surface of TMDC-NDs and their interface with graphene is important to obtain higher photoresponse and speed. Figure S5c (Supporting Information) compares the dynamic photoresponse measured on the WMW-NDs/graphene sample immediately after the sample was made and 5 days later. A degradation of photoresponse around 55% was observed, indicating leaving the sample in ambient is harmful. To further probe the stability, the photoresponse on a continuous single layer of MoS_2 and a bilayer of MoS_2/graphene nanohybrids were followed over a period of eight months, and the result is summarized in Figure S6 (Supporting Information). Specifically, Figure S6a–c (Supporting Information) exhibits the photoresponse over time measured on three different channels of MoS_2 single layer and Figure S6d–f (Supporting Information), of MoS_2/graphene bilayers. Lights of different wavelengths of 400, 550, 700, 850, and 1000 nm were used in the characterization. Note the photoresponse is about 3 orders of magnitude higher in the latter due to the photoconductive gain introduced by graphene. During the test time of about 240 days (≈8 months), a decrease in the photoresponse can be observed on both of the samples. In the MoS_2 only sample, the decrease is ≈30–40% over the 240-day period while in the bilayer sample, a more severe decrease occurred in the photoresponse by up to an order of magnitude (channels 1 and 3). Interestingly, Channel 2 experienced smaller decrease of ≈60–70% within the first 30 days, followed with more or less constant photoresponse in the 7 months afterwards. This sample-to-sample variation of the stability suggests that precautions may be developed to reduce the degradation of the MoS_2 in ambient.

The photoresponsivity (R) is an important parameter for a photodetector and can be calculated from the ratio between photocurrent (I_{ph}) and incident light power. The I_{ph} is defined as the difference between the device current under illumination (I_{light}) and in dark (I_{dark}): $I_{ph} = I_{light} - I_{dark}$. Quantitatively, R is defined as[28]

$$R = \frac{I_{ph}}{P_{in}} \quad (1)$$

where P_{in} is the illumination intensity. Figure 6d compares the R values measured on three TMDC-NDs/graphene vdW nanohybrids photodetectors including M-NDs/graphene (green), WM-NDs/graphene (black), and WMW-NDs/graphene (blue) as function of P_{in}. The R values of all three devices increase monotonically with decreasing P_{in} as reported in nanohybrids photodetectors.[29] The highest R-value of 10.5 A/W was obtained on the WMW-NDs/graphene device at the lowest P_{in} ≈12 μW cm^{-2}, which is 3.2 times of that on the M-NDs/graphene device.

Figure S7 (Supporting Information) compares the photoresponsivity of three TMDC/graphene nanohybrids with different TMDC morphologies including: WMW-NDs (blue), MoS_2-NDs (green), and WS_2-continuous layer (red).[30] The WMW-NDs/graphene exhibits the highest R values up to 10.5 A/W) due to the optimal WMW-NDs density of 1.1 ± 0.1 particles μm^{-2} and lateral ND size of 400–600 nm. In the case of the MoS_2-NDs/graphene, a smaller concentration of NDs ≈0.43 particles μm^{-2} leads to lower R values (≈3.4 A/W at the lowest light intensity). The lowest measured R values up to 0.2 A/W were found on the WS_2-continuous layer/graphene sample,[30] which illustrates the benefits of the LSPR induced in TMDC-NDs.

Figure 7a shows the R values as function of TMDC-NDs concentration on four samples of MW-NDs/graphene, WM-NDs/graphene, MWM-NDs/graphene, and WMW-NDs/graphene. The monotonically increasing R-value with increasing concentration of TMDCs-NDs confirms the enhanced light absorption at a higher concentration of TMDC-NDs. The WMW-NDs/graphene nanohybrids photodetector was further investigated as the highest ND concentration was found in this sample. Figure S8a (Supporting Information) shows the dynamic photocurrent on photodetector response to light on and off (550 nm in wavelength and 0.39 mW in light power) at different V_{sd} values of 1.0, 1.5, 2.0, and 2.5 V. Figure S8b (Supporting Information) demonstrates the R versus V_{sd} curve extracted from Figure S8a (Supporting Information), showing that the R-value increases approximately linearly with V_{sd} because of the increase in carrier drift velocity. The time constant t_{rise} and t_{fall} are ≈0.1–0.2 s, which is better than the 3.2–1.2 s reported on MoS_2/graphene nanohybrids with transferred MoS_2.[28] Figure 7b displays the R values as a function of incident light intensity measured on the WMW-NDs/graphene photodetector at V_{sd} = 2.5 V. The R values decrease with increasing incident power and the highest R ≈31 A/W (550 nm wavelength and 20 μW cm^{-2} light intensity) was achieved on the device.

Figure 8a displays the dynamic photoresponse of the WMW-NDs/graphene photodetector measured in response to lights of different wavelengths in the range of 400 to 900 nm. The source-drain bias voltage was maintained at 1.0 V. The device exhibits photoresponse to all wavelengths. A similar measurement was carried out on a M-NDs/graphene device for the purpose of comparison. Figure 8b compares the calculated R values as a function of wavelength on these two photodetectors. Overall, the WMW-NDs/graphene photodetector shows considerably higher R values over the entire wavelength range of 400–900 nm than its M-NDs/graphene counterpart's. Considering the two devices have otherwise the same structure except TMDC-NDs of different concentrations, the enhanced photoresponsivity is most probably attributed to the higher density of the TMDC-NDs in the WMW-NDs/graphene photodetector. Furthermore, a broad peak

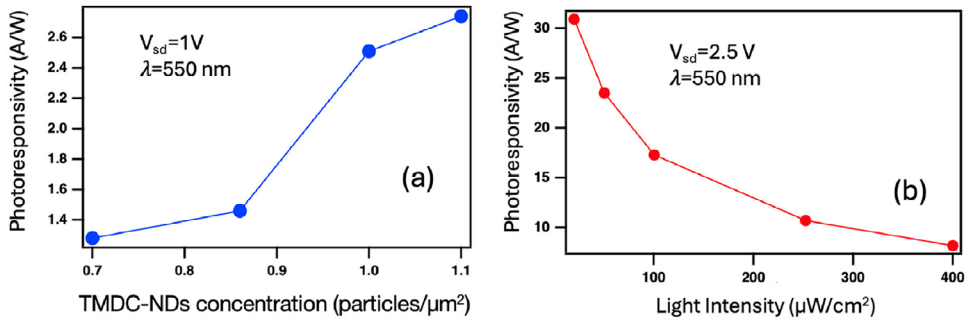

Figure 7. a) Photoresponsivity as a function of TMDC-NDs concentration for the four TMDC-NDs/graphene nanohybrid samples of intermingled WM-NDs, MW-NDs, MWM-NDs, and WMW-NDs on the right of Figure 5. Incident light of 550 nm wavelength and 400 μW cm^{-2} light intensity was used for the test. b) Photoresponsivity as a function of the incident light intensity on the WMW-NDs/graphene photodetector (V_{sd} is 2.5 V).

of photoresponsivity located in the range of 450–600 nm and a smaller one located >650 nm on the WMW-NDs/graphene device likely corresponding the LSPR wavelength of the WS_2-NDs and MoS_2-NDs, respectively. A similar result was reported on WS_2-ND with LSPR peak located between 450–575 nm.[21] Figure 8c displays the reduction of the photoresponse as the light power was reduced in the range of 20–250, 24–300, and 20–252 μW cm^{-2} at three different wavelengths of 550, 650, and 750 nm respectively, and V_{sd} = 2.5 V. Figure 8d demonstrates the calculated R values as a function of light intensity for the three wavelengths. A similar increasing R-value with decreasing light intensity trend can be observed for all three wavelengths. Quantitatively, R values of 31 A/W (550 nm wavelength and 20 μW/cm^2 light intensity), 27 A/W (650 nm wavelength and 24 μW cm^{-2} light intensity), and 43 A/W (750 nm wavelength and 20 μW cm^{-2} light intensity) have been obtained on this device.

2. Conclusion

In conclusion, this work presents a study to synthesize TMDC-NDs of high LSPR effect (specifically MoS_2 and WS_2) with controllable ND dimension and concentration on graphene using a wafer-size, solution-coating process followed by vapor transport annealing in sulfur vapor. It should be noted that the LSPR effect induced uniquely on the TMDC-NDs allows significantly enhanced light absorption than in their TMDC continuous layer counterpart in which the LSPR is negligible.[20b,21] However, the LSPR effect on TMDC-NDs is affected sensitively by the ND dimension and the concentration, which motivated this study. Several important insights have been obtained. First, TMDC-NDs can form if the TMDC precursor coating, specifically $(NH_4)_2MoS_4$ and $(NH_4)_2WS_4$, is highly diluted to below 0.26 wt.%. On the other hand, multiple coatings of the

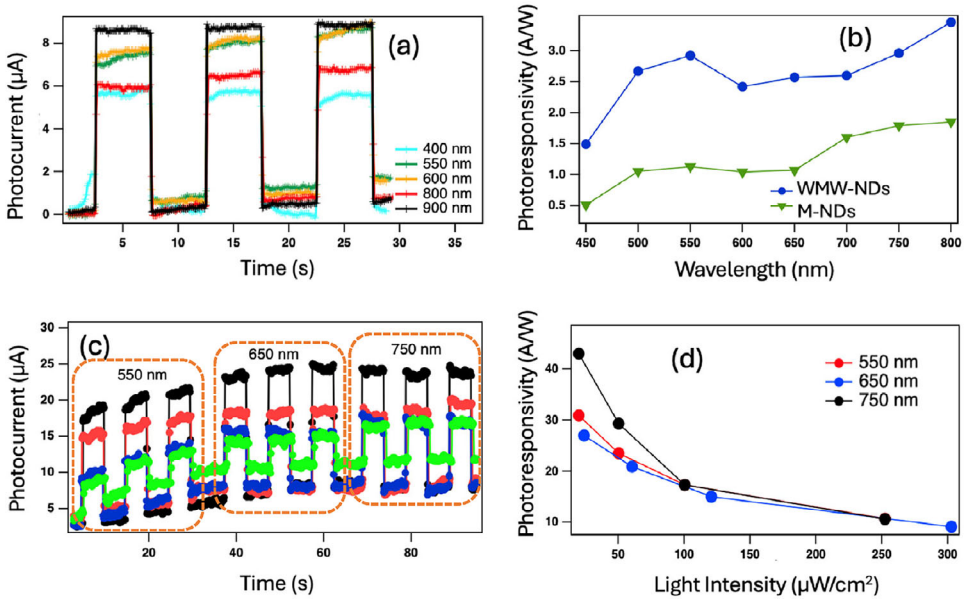

Figure 8. a) Dynamic photoresponse of a representative WMW-NDs/graphene photodetector measured in response to lights of different wavelengths in the range of 400–900 nm. b) Comparison of the spectral photoresponsivity of the WMW-NDs/graphene (blue) and MoS_2-NDs/graphene (green) photodetectors. c) Dynamic photoresponse of the WMW-NDs/graphene photodetector measured at wavelengths of 550, 650, and 750 nm with variable incident optical intensities in the range of 20–250, 24–300, and 20–252 μW cm^{-2} respectively. d) The corresponding photoresponsivity of the WMW-NDs/graphene photodetector as a function of light intensity.

same kinds of TMDC were found ineffective to generate small-dimension and high-concentration TMDC-NDs. This may be associated to the nucleation of the TMDC-NDs in the additional coating on the same kind of TMDC-NDs formed from previous coating(s), leading to larger and thicker NDs instead of a higher ND concentration of unchanged ND dimension. Finally, consecutive coatings of different kinds of TMDCs allows circumvention of the problem, leading to formation of small-dimension and high-concentration intermingled NDs of different kinds of TMDCs. On the TMDC-NDs/graphene nanohybrids photodetectors, a monotonically increasing photoresponse with increasing TMDC-NDs concentration has been observed in visible spectrum. In the WMW-NDs/graphene nanohybrids made with three consecutive coatings of WS_2-NDs (1st and 3rd coating) and MoS_2 (2nd coating) with the highest TMDC-NDs concentration of 1.1 ± 0.1 particles μm^{-2} that is almost 8.5 times higher than that in the W-NDs/graphene sample (0.13 ± 0.03 particles μm^{-2}). The high ND concentration together with the suitable ND dimension in the range of 400–600 nm in the WMW-NDs/graphene device plays a critical role to achieve high LSPR effect and light absorption. This leads to high *R* values of 31 A/W (550 nm wavelength and 20 μW cm^{-2} light intensity), 27 A/W (650 nm wavelength and 24 μW cm^{-2} light intensity), and 43 A/W (750 nm wavelength and 20 μW cm^{-2} light intensity) on the WMW-NDs/graphene photodetector.

3. Experimental Section

Growth of Graphene Using Chemical Vapor Deposition (CVD): The growth of graphene was carried out inside a quartz tube placed inside CVD system. The details of the synthesis procedure have been explained in detail in our earlier works.[31] Briefly, graphene was synthesized on the copper foil (25 μm thick) positioned inside a quartz tubular reactor in the flow of a mixed gas of H_2 (7 sccm) and CH_4 (40 sccm) in the CVD furnace at 1050 °C. The growth time was ≈30 min. A wet transfer procedure was used to transfer graphene on SiO_2 /Si substrates. [31] 3% Poly(methyl methacrylate) (PMMA) was spin-coated on top of the graphene/Cu sample (at 3000 rpm for around 30 s). Then, the sample was heated on hotplate at 120 °C for ≈5 min. After that, the sample was soaked into copper etchant (Ferric chloride solution $FeCl_3$) for ≈4 h to remove the Cu foil. The PMMA/graphene samples were then rinsed a few times with deionized water. Afterward, the PMMA/graphene samples were placed on SiO_2/Si substrate and left overnight to dry at room temperature in ambient. Finally, the PMMA/graphene/SiO_2/Si was soaked in acetone roughly four times to dissolve the PMMA.

Fabrication of TMDC-ND/Graphene vdW Nanohybrids Photodetectors: TMDC-NDs were directly grown on graphene/SiO_2/Si with prefabricated Au/Ti source and drain electrodes. Electron-beam evaporation was used to deposit the electrodes of Au/Ti (40 nm/10 nm) through a metal shadow mask. The defined channel length between the two electrodes was ≈ 250 μm and the channel width was in the range of 2–3 mm. Two kinds of TMDC-NDs, namely MoS_2-NDs, and WS_2-NDs, were synthesized on graphene using a vapor transport process developed in our earlier works.[22] To obtain the intermingled WS_2-NDs and MoS_2-NDs, these two kinds of TMDCs were grown consecutively on graphene after removing the PMMA. For the MoS_2 growth, a precursor solution of $(NH_4)_2MoS_4$ was first synthesized via dissolving $(NH_4)_2MoS_4$ powder in N,N-dimethylformamide (DMF). The precursor concentration was found critical in controlling the morphology of the MoS_2. Specifically, when the precursor concentration was varied from 0.06 to 0.40 wt.%, the MoS_2 exhibits NDs at lower concentrations and nano-donuts at higher concentrations.[32] Therefore, a low concentration of 0.26 wt.% was selected in this work to generate NDs. In addition, it was found that adding more coatings of the same kinds of TMDC precursors, even at low precursor concentrations, would lead to larger and irregular shaped NDs that evolve eventually to a continuous, multilayered sheet of TMDCs with three to four coatings of the same kind of TMDCs. [22b] The graphene/SiO_2/Si or SiO_2/Si were dipped in the precursor solution, followed with spinning at 3000 rpm for 60 s to spread the precursor uniformly on the substrates. In order to obtain this TMDC-ND morphology, the small precursor coating thickness and the coating number were important.[22b] At larger precursor thicknesses, TMDC will grow in continuous layers. After approximately 3 to 4 coatings of the low-concentration precursor, a continuous TMDC layer would be generated by increasing the TMDC-ND concentration and the dimension.[22b] Afterward, the samples were annealed in the flow of a mixed gas Ar (40 sccm) and H_2 (10 sccm)) at 450 °C for 30 min in sulfur vapor transported from the sulfur powder positioned upstream from the sample in a quartz tube at ≈200 °C. The pressure was maintained at ≈50 mTorr throughout the MoS_2 growth. The growth procedure for WS_2 was similar except the ammonium tetrathiotungstate $(NH_4)_2WS_4$ precursor was adopted. In order to obtain higher concentration of the TMDC-NDs, two approaches were explored in this work. One is to repeat the growth procedure for one kind of TMDCs (MoS_2 or WS_2) several times and the other, two different kinds alternatively. For convenience of the notation, "M" and "W" were used respectively for samples with multiple coatings of MoS_2 and WS_2. For example, a sample with intermingled TMDC-NDs generated from three coatings of MoS_2 (1st coating), WS_2 (2nd coating), and MoS_2 (3rd coating) will be regarded as "MWM" in the following discussions.

Characterization of TMDC-NDs/Graphene Photodetectors: Raman spectra and Raman maps of graphene and TMDCs were collected using a Witec Alpha300-Confocal Raman microscope. AFM images were collected using a Digital Instruments Multimode Nanoscope IIIA AFM system in contact mode using standard silicon nitride cantilevers (k = 0.06, 0.27 N m^{-1}). CHI660D electrochemical workstation was used to measure the current–voltage (*I*–*V*) characteristics of the photodetectors. The dynamic photocurrent measurements in visible spectrum were performed using an Oriel Apex monochromator illuminator with different bias voltages in the range of 1.0 – 2.5 V across the source and drain electrodes.

Supporting Information

Supporting Information is available from the Wiley Online Library or from the author.

Acknowledgements

This scientific paper was derived from a research grant funded by the Research, Development, and Innovation Authority (RDIA) – Kingdom of Saudi Arabia – with grant number (12894-JAZZAN-2023-JZU-R-2-1-SE). Additionally, this research was supported by the US National Science Foundation through grants of NSF ECCS-2412221 and NSF-2322053.

Conflict of Interest

The authors declare no conflict of interest.

Data Availability Statement

The data that support the findings of this study are available on request from the corresponding author. The data are not publicly available due to privacy or ethical restrictions.

Keywords

nanohybrids, optoelectronics, photodetectors, plasmonic, TMDC nanodiscs

Received: February 7, 2025
Revised: March 28, 2025
Published online:

[1] a) S. Li, X. Liu, H. Yang, H. Zhu, X. Fang, *Nat. Electron.* **2024**, *7*, 216; b) H. Chen, L. Su, M. Jiang, X. Fang, *Adv. Funct. Mater.* **2017**, *27*, 1704181; c) J. Y. Lee, J.-H. Shin, G.-H. Lee, C.-H. Lee, *Nanomaterials.* **2016**, *6*, 193; d) G. Eda, S. A. Maier, *ACS Nano.* **2013**, *7*, 5660; e) J. Z. Wu, S. A. Ghopry, B. Liu, A. Shultz, *Micromachines.* **2023**, *14*, 1393.

[2] a) I. Song, C. Park, H. C. Choi, *RSC Adv.* **2015**, *5*, 7495; b) Z. Yin, H. Li, H. Li, L. Jiang, Y. Shi, Y. Sun, G. Lu, Q. Zhang, X. Chen, H. Zhang, *ACS Nano.* **2012**, *6*, 74.

[3] a) K. Yang, T. Liu, X.-D. Zhang, *Front. Chem.* **2021**, *9*, 700250; b) D. Haldar, A. Ghosh, U. K. Ghorai, S. K. Saha, *Mater. Res. Bull.* **2020**, *129*, 110879.

[4] a) K. F. Mak, C. Lee, J. Hone, J. Shan, T. F. Heinz, *Phys. Rev. Lett.* **2010**, *105*, 136805; b) Y. Zhang, T.-R. Chang, B.o Zhou, Y.-T. Cui, H. Yan, Z. Liu, F. Schmitt, J. Lee, R. Moore, Y. Chen, H. Lin, H.-T. Jeng, S.-K. Mo, Z. Hussain, A. Bansil, Z.-X. Shen, *Nat. Nanotechnol.* **2014**, *9*, 111; c) D.o Muoi, N. N. Hieu, H. T. T. Phung, H. V. Phuc, B. Amin, B. D. Hoi, N. V. Hieu, L. C. Nhan, C. V. Nguyen, P. T. T. Le, *Chem. Phys.* **2019**, *519*, 69.

[5] U. Ahuja, A. Dashora, H. Tiwari, D. C. Kothari, K. Venugopalan, *Comput. Mater. Sci.* **2014**, *92*, 451.

[6] A. K. Geim, K. S. Novoselov, *Nat. Mater.* **2007**, *6*, 183.

[7] a) J.-H. Chen, C. Jang, S. Xiao, M. Ishigami, M. S. Fuhrer, *Nat. Nanotechnol.* **2008**, *3*, 206; b) C. R. Dean, A. F. Young, I. Meric, C. Lee, L. Wang, S. Sorgenfrei, K. Watanabe, T. Taniguchi, P. Kim, K. L. Shepard, J. Hone, *Nat. Nanotechnol.* **2010**, *5*, 722.

[8] a) A. K. Geim, *Science.* **2009**, *324*, 1530; b) R. R. Nair, P. Blake, A. N. Grigorenko, K. S. Novoselov, T. J. Booth, T. Stauber, N. M. R. Peres, A. K. Geim, *Science.* **2008**, *320*, 1308.

[9] a) P. S. Sachidanand, M. M. Sreelal, S. Reshmi, G. Viswan, M. Mohan, S. K. Gautam, R. K. Singh, K. Bhattacharjee, *Mater. Today Proc.* **2020**, *26*, 104; b) V. Raman, D. Rhee, A. R. Selvaraj, J. Kim, K. Prabakar, J. Kang, H.-K.i Kim, *Sci. Technol. Adv. Mater. 22*, 875; c) J. Yoon, W. Park, G.-Y. Bae, Y. Kim, H. S. Jang, Y. Hyun, S. K. Lim, Y. H. Kahng, W.-K. Hong, B. H. Lee, H. C. Ko, *Small.* **2013**, *9*, 3295.

[10] C. Lan, C. Li, Y. Yin, Y. Liu, *Nanoscale.* **2015**, *7*, 17980.

[11] a) K. Kang, K. H. Lee, Y. Han, et al., *Nature.* **2017**, *550*, 229; b) P. Rivera, K. L. Seyler, H. Yu, J. R. Schaibley, J. Yan, D. G. Mandrus, W. Yao, X. Xu, *Science.* **2016**, *351*, 688; c) K. S. Thygesen, *2D Mater.* **2017**, *4*, 022004; d) N. R. Wilson, P. V. Nguyen, K. Seyler, P. Rivera, A. J. Marsden, Z. P. L. Laker, G. C. Constantinescu, V. Kandyba, A. Barinov, N. D. M. Hine, X. Xu, D. H. Cobden, *Sci. Adv.* **2017**, *3*, 1601832; e) F. Barati, M. Grossnickle, S. Su, R. K. Lake, V. Aji, N. M. Gabor, *Nat. Nanotechnol.* **2017**, *12*, 1134; f) M. Massicotte, P. Schmidt, F. Vialla, et al., *Nat. Nanotechnol.* **2016**, *11*, 42.

[12] a) A. Pezeshki, S. H. H. Shokouh, T. Nazari, K. Oh, S. Im, *Adv. Mater.* **2016**, *28*, 3216; b) K. Zhang, T. Zhang, G. Cheng, T. Li, S. Wang, W. Wei, X. Zhou, W. Yu, Y. Sun, P. Wang, D. Zhang, C. Zeng, X. Wang, W. Hu, H. J. Fan, G. Shen, X. Chen, X. Duan, K. Chang, N. Dai, *ACS Nano.* **2016**, *10*, 3852.

[13] R. Cheng, D. Li, H. Zhou, C. Wang, A. Yin, S. Jiang, Y. Liu, Y. Chen, Y. Huang, X. Duan, *Nano Lett.* **2014**, *14*, 5590.

[14] a) Y. Wang, W.-X. Zhou, L. Huang, C. Xia, L. M. Tang, H. X. Deng, Y. Li, K. Q. Chen, J. Li, Z. Wei, *2D Mater.* **2017**, *4*, 025097; b) T. Yang, B. Zheng, Z. Wang, T. Xu, C. Pan, J. Zou, X. Zhang, Z. Qi, H. Liu, Y. Feng, W. Hu, F. Miao, L. Sun, X. Duan, A. Pan, *Nat. Commun.* **2017**, *8*, 1906.

[15] a) Y. Deng, Z. Luo, N. J. Conrad, H. Liu, Y. Gong, S. Najmaei, P. M. Ajayan, J. Lou, X. Xu, P. D. Ye, *ACS Nano. 8*, 8292; b) L. Ye, H. Li, Z. Chen, J. Xu, *ACS Photonics.* **2016**, *3*, 692.

[16] T. Qi, Y. Gong, A. Li, X. Ma, P. Wang, R. Huang, C. Liu, R. Sakidja, J. Z. Wu, R. Chen, L. Zhang, *Adv. Funct. Mater.* **2020**, *30*, 1905687.

[17] Y. Xue, Y. Zhang, Y. Liu, H. Liu, J. Song, J. Sophia, J. Liu, Z. Xu, Q. Xu, Z. Wang, J. Zheng, Y. Liu, S. Li, Q. Bao, *ACS Nano.* **2016**, *10*, 573.

[18] A. Li, Q. Chen, P. Wang, Y. Gan, T. Qi, P. Wang, F. Tang, J. Z. Wu, R. Chen, L. Zhang, Y. Gong, *Adv. Mater.* **2019**, *31*, 1805656.

[19] G. Konstantatos, M. Badioli, L. Gaudreau, J. Osmond, M. Bernechea, F. P. G. de Arquer, F. Gatti, F. H. L. Koppens, *Nat. Nanotechnol.* **2012**, *7*, 363.

[20] a) C. Lan, C. Li, S. Wang, et al., *J. Mater. Chem. C.* **2017**, 5,; b) Q. Liu, B. Cook, M. Gong, Y. Gong, D. Ewing, M. Casper, A. Stramel, J. Wu, *ACS Appl. Mater. Interfaces.* **2017**, *9*, 12728.

[21] M. Alamri, M. Gong, B. Cook, R. Goul, J. Z. Wu, *ACS Appl. Mater. Interfaces.* **2019**, *11*, 33390.

[22] a) S. A. Ghopry, M. Alamri, R. Goul, B. Cook, S. M. Sadeghi, R. R. Gutha, R. Sakidja, J. Z. Wu, *ACS Appl. Nano Mater.* **2020**, *3*, 2354; b) S. A. Ghopry, M. A. Alamri, R. Goul, R. Sakidja, J. Z. Wu, *Adv. Opt. Mater.* **2019**, *7*, 1801249.

[23] a) R. Lu, A. Konzelmann, F. Xu, Y. Gong, J. Liu, Q. Liu, M. Xin, R. Hui, J. Z. Wu, *Carbon.* **2015**, *86*, 78; b) A. Mahigir, T.e-W. Chang, A. Behnam, G. L. Liu, M. R. Gartia, G. Veronis, *Sci. Rep.* **2017**, *7*, 14044; c) S. G. Zhang, X. W. Zhang, X. Liu, Z. G. Yin, H. L. Wang, H. L. Gao, Y. J. Zhao, *Appl. Phys. Lett.* **2014**, *104*, 121109.

[24] a) H. E. Romero, N. Shen, P. Joshi, H. R. Gutierrez, S. A. Tadigadapa, J. O. Sofo, P. C. Eklund, *ACS Nano.* **2008**, *2*, 2037; b) X. Wang, X. Li, L.i Zhang, Y. Yoon, P. K. Weber, H. Wang, J. Guo, H. Dai, *Science.* **2009**, *324*, 768.

[25] J. Z. Wu, M. Gong, *Adv. Photonics Res.* **2021**, *2*, 2100015.

[26] N. V. Joshi, *Photoconductivity: art, science, and technology*, Marcel Dekker, New York **1990**.

[27] H. Xu, J. Wu, Q. Feng, N. Mao, C. Wang, J. Zhang, *Small.* **2014**, *10*, 2300.

[28] B.o Sun, T. Shi, Z. Liu, Y. Wu, J. Zhou, G. Liao, *Mater. Des.* **2018**, *154*, 1.

[29] J. Z. Wu, M. Gong, N. Photodetectors, *Adv Photon Res.* **2021**, *2*, 2100015.

[30] M. Alamri, R. Sakidja, R. Goul, S. Ghopry, J. Z. Wu, *ACS Appl. Nano Mater.* **2019**, *2*, 1412.

[31] a) B. Cook, Q. Liu, J. Liu, M. Gong, D. Ewing, M. Casper, A. Stramel, J. Wu, *J. Mater. Chem. C.* **2017**, *5*, 10087; b) M. Gong, Q. Liu, B. Cook, B. Kattel, T.i Wang, W.-L. Chan, D. Ewing, M. Casper, A. Stramel, J. Z. Wu, *ACS Nano.* **2017**, *11*, 4114.

[32] S. A. Ghopry, S. M. Sadeghi, C. L. Berrie, J. Z. Wu, *Biosensors.* **2021**, *11*, 477.